(22) Stepto, R. T. F. In *Developments in Polymerization. 3*; Haward, R. N., Ed.; Applied Science Publishers: Barking, U.K., 1982; p 81.
(23) Kuchanov, S. I. *Methods of kinetic calculations in polymer chemistry (in Russian)*; Khimia: Moscow, 1978.
(24) Kuchanov, S. I.; Povolotskaya, E. S. *Vysokomol. Soedin, Ser. A* **1982**, *24*, 2179.
(25) Dušek, K. *Br. Polym. J.* **1985**, *17*, 185.
(26) Spouge, J. L. *Macromolecules* **1983**, *16*, 121.
(27) Mikeš, J.; Dušek, K. *Macromolecules* **1982**, *15*, 93.
(28) Kuchanov, S. I.; Povolotskaya, E. S. *Vysokomol. Soedin., Ser. A* **1982**, *24*, 2190.
(29) Galina, H.; Szustalewicz, A. *Macromolecules* **1989**, *22*, 3124.
(30) Galina, H. *Europhys. Lett.* **1987**, *3*, 1155.
(31) Smoluchowski, M. V. *Phys. Z.* **1916**, *17*, 585.
(32) Hairer, E.; Nørsett, S. P.; Wanner, G. *Solving Ordinary Differential Equations. I. Non-stiff problems*; Springer: Berlin, 1987.
(33) Stockmayer, W. H. *J. Polym. Sci.* **1952**, *9*, 69; **1953**, *11*, 424.
(34) Galina, H.; Kennedy, J. W.; Quintas, L. V., to be submitted for publication.

Size Effect of Compliant Rubbery Particles on Craze Plasticity in Polystyrene

E. Piorkowska,† A. S. Argon,* and R. E. Cohen

Massachusetts Institute of Technology, Cambridge, Massachusetts 02139

Received November 13, 1989; Revised Manuscript Received January 30, 1990

ABSTRACT: Blends of polystyrene containing concentric spherical shell particles produced from KRO-1 resin by means of a morphological transformation discussed earlier by Gebizlioglu et al.[7] were disassembled to harvest the particles. These particles were in turn separated into two nearly nonoverlapping populations of average sizes of 0.32 and 2.3 μm and were subsequently reassembled by solvent blending into homo-PS to create two separate sets of heterogeneous polymers of large and small particles at particle weight fractions of 0.05 and 0.15, respectively. It was found that the craze flow stress increases systematically with decreasing particle volume fraction at constant particle size and that the blends with the small particles that are less potent craze initiators have substantially higher flow stresses than blends with the large particles. Definitive theoretical models for the cutoff particle size below which crazes cannot be initiated and for the craze flow stress are in substantial agreement not only with the results of the present study but also with particle size effects previously reported by us and other investigators.

I. Introduction

The incorporation of rubber particles with certain morphology into a normally brittle glassy polymer can substantially increase its toughness.[1-3] This approach has been used for decades in the production of tough polymers such as high-impact polystyrene (HIPS) or acrylonitrile–butadiene–styrene (ABS). In these polymers the particles act as potent craze initiators, and the source of the toughness is the extensive dilatational plasticity that results from the initiated crazes.[4,5] It has been stated that for particles to be effective they must be very compliant, must have a size exceeding a critical value, and finally, must be adhering well to the surrounding glassy polymer so they can eventually become fully load bearing when that becomes necessary.

Recent studies conducted on blends of polystyrene with polystyrene/polybutadiene (PS/PB) copolymers by Gebizlioglu et al.[6,7] have shown that the effectiveness of particles as craze initiators is governed not only by rubber content but even more importantly by particle morphology. The incorporation of low molecular weight PB into the KRO-1 type PS/PB block copolymer particles transformed their morphology from randomly interwoven rods of PB embedded in PS to a morphology comprised of concentric spherical shells of PS and PB. This morphological transformation accomplished by a small addition of rubber was found to result in a large increase of particle compliance and therefore in a significant increase of toughness.[6,7]

The effect of particle size on the mechanical properties of rubber-toughened polymers has been studied by a number of investigators.[1,3,8-11] There is agreement that rubber particles of a size less than some critical value are ineffective as craze initiators.[1,3] The critical size of particles, however, depends on the mechanical properties of both the matrix and the particles. Most studies of particle size effect on rubber-toughened PS concern mainly HIPS. Boyer and Keskkula[9] found that the optimum particle size for HIPS is within the range 1–2 μm, while Donald and Kramer[10] reported that particles of diameter <0.8 μm do not initiate crazes in HIPS. Bragaw[3] stated that particle size should be larger than the thickness of a craze to be effective as craze initiators. Similar observations concern also PS toughened with block copolymer particles of PS/PB. For such systems Gebizlioglu et al.[6,7] determined that particles of diameter less than a critical value do not initiate crazes but found that the critical cutoff size ranged from 0.1 to 0.4 μm for concentric spherical shell particles, while KRO-1 particles of much higher stiffness did not appear to initiate crazes even when exceeding 10 μm in size.

Uncertainty in the determination of the role of the particle size on toughening of the glassy matrix originates from the difficulties of controlling particle size without

† Permanent address: Centre of Molecular and Macromolecular Studies, Polish Academy of Sciences, 90-362 Lodz, Poland.

0024-9297/90/2223-3838$02.50/0

affecting other important parameters such as rubber content, particle chemistry, morphology, or the state of its bonding to the matrix. Previous evaluations of the role of particle size have come from studies of materials differing not only in particle size but also in some or all of the important parameters mentioned above. Therefore, their accuracy is questionable.

Information about the effect of particle size on toughening has often been obtained from determinations of the number of crazes generated by particles of various sizes. These crazes have been viewed in cross-sections of samples containing particles with a broad distribution of sizes. In such observations it is not always clear if the crazes have been initiated by the particles or merely encounter them in their path. It is also possible that particles in the borderline range of criticality may behave differently if unaccompanied by larger ones.

In the present paper we report the results of a study of the toughness of blends of polystyrene with spherical shell particles composed of alternating shells of PS and lightly cross-linked PB. Two materials were prepared differing only in particle size, while maintaining the same particle morphology, chemistry, and PB volume fraction. These particles were chosen since they are known to be very efficient craze initiators.[7,12] Particles having this morphology were formed within a PS matrix from a PS/PB block copolymer blended with additional PB of molecular weight lower than that of the PB block of the copolymer.[7,12] By employment of two different rates of casting of films from the same polymer solution, two source materials containing two sets of particles were obtained. One source material with particles of sizes up to 4.5 μm was obtained by spin casting, while another with particles of sizes only up to 0.6 μm was prepared by static casting. Particles in both sets had the same composition, the same concentric spherical shell (CSS) morphology, and, therefore, almost the same mechanical properties. Significant differences in thickness of the two samples, on the one hand, and important gradients of average particle size across the sample thickness for the case of the films with smaller particles together with relatively low content of particles in these samples, on the other hand, made the as-cast films inappropriate for direct studies. Therefore, these original films were used only as source materials for harvesting particles of two separate size distributions.

Prior to the harvesting of these particles to obtain narrow size distributions in a way described in section II, the cast film samples were annealed under vacuum at a temperature slightly above T_g of PS. After exposure to high-energy electron irradiation, the PS matrices of the two source samples were dissolved, leading to suspensions of swollen CSS particles in dilute PS solution. The jelly-like particles were carefully separated from the solution by means of centrifugation and were reincorporated into a new PS solution at the desired particle concentration. A standard casting method was then applied to all samples made from these suspensions. This procedure led to film samples differing only in sizes of CSS particles but otherwise having identical properties. Samples of different controlled volume fractions of particles of narrow size distributions could thus be prepared. The tensile properties as well as morphology of these samples were studied in considerable detail as reported below.

The important experimental details on how source materials with concentric spherical shell particles were obtained, how they were processed and disassembled to collect particles, and how these particles were separated into different size ranges and were again reassembled into new blends by solvent processing to obtain material with tighter particle size distributions will not be given in the text so as not to divert the attention of the reader. All of this detail, including also morphology examinations and tensile testing, can be found in Appendix I.

II. Experimental Results

2.1. Samples with Tight Particle Size Distributions. The samples used as particle sources prepared by spin casting and static casting were spot checked by transmission electron microscopy (TEM) to establish that they contained the expected spherical shell particles. Figure 1a shows the TEM micrograph of an ultrathin section of the 0.5-mm-thick spin-cast sample of source material with large particles. No separate PB inclusions were found. Particles were randomly distributed across the sample thickness. The maximum particle size did not exceed 4.5 μm. The frequency distribution of the volume fraction of particles according to size in the original spin-cast source films was determined by SEM and was found to range from 0.1 to above 5 μm in this source material as shown in Figure 2. The particles obtained from these spin-cast samples will be referred to as the large-particle population. The majority of the total volume fraction of particles in this material was distributed between diameters from 1.5 to 3.5 μm, with a population average particle size of 2.46 μm. The 0.13-mm-thick static-cast samples were found to have particles of sizes changing gradually across the sample thickness. However, particle diameters in these samples did not exceed 0.6 μm. Thus the particles obtained from these static-cast samples will be referred to as the small-particle population. Figure 1b shows the structure of the static-cast film close to the substrate on which it was cast. All particles in this sample also had well-developed CSS morphology.

The 30-Mrad dose of electron irradiation enabled particles to remain intact after dissolution of source samples and reincorporation into new blends. Figure 3 shows a comparison of results of tensile tests conducted on spin-cast samples having 21.7 wt % of KRO-1/PB-6K particles before (solid curve) and after (dashed curve) electron irradiation with a dose of 30 Mrad. Clearly, the irradiation that was necessary to make the particles survive the disassembly process by dissolving the matrix PS increases the flow stress somewhat and decreases the elongation, but substantial plastic straining still occurs, which indicates the presence of extensive craze plasticity. Therefore, it was concluded that the irradiated particles do not lose their ability to initiate crazes to any significant degree.

It was found that 3 h of centrifugation at $9.6 \times 10^4 g$ at 20 °C leads to separation of irradiated cross-linked particles from the dissolved polystyrene matrix. Figure 4 shows the TEM micrograph of an ultrathin film cast from a resuspended sediment collected after centrifugation of the dissolved static-cast sample having 5 wt % of KRO-1/PB-6K particles of sizes up to 0.6 μm. It is seen that the sediment consists entirely of the CSS particles with undisturbed morphology. In the case of this sample approximately 30% of the total particle content was collected after centrifugation. The rest of the particles remained in the suspension due to their small sizes and inability to settle under these centrifugation conditions within the given time. In the case of the spin-cast sample containing particles of sizes up to 4.5 μm, the weight of collected particles was approximately equal to the total content of particles, with only a very small fraction of the smallest particles remaining in the suspension.

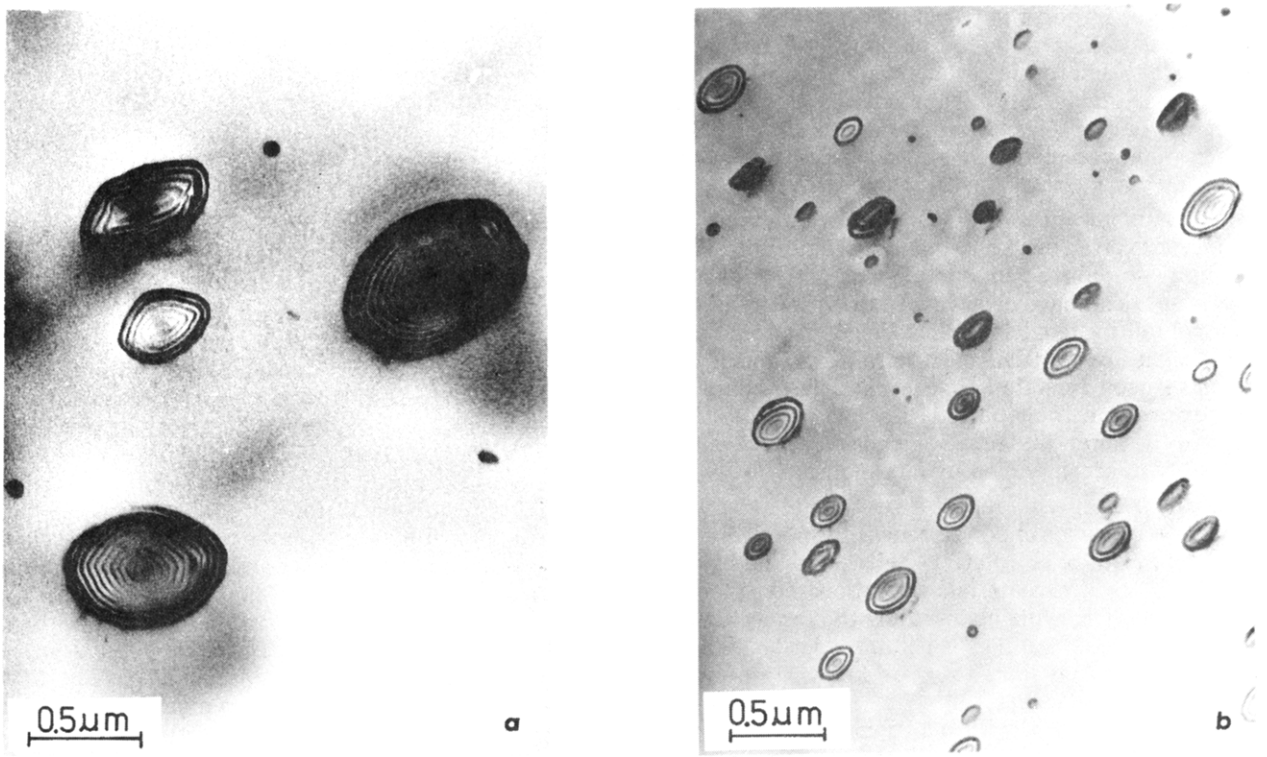

Figure 1. TEM micrographs of ultrathin sections of the samples containing 5 wt % of KRO-1/PB-6K particles: (a) spin-cast sample; (b) static-cast sample, area close to the lower surface of the film.

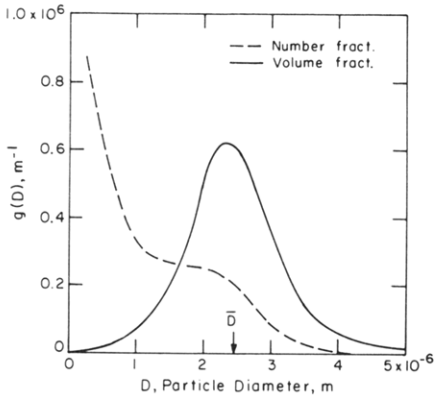

Figure 2. Number and volume fraction distributions of sizes of particles formed in the original spin-cast sample containing 5 wt % of KRO-1/PB-6K particles.

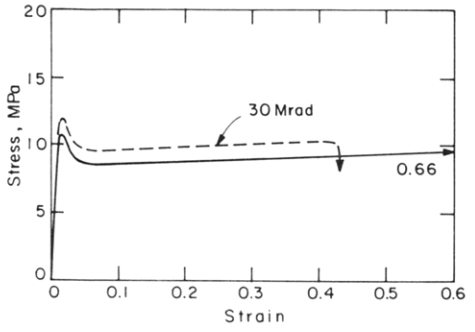

Figure 3. Stress–strain behavior of spin-cast, annealed samples containing 21.7 wt % of KRO-1/PB-6K particles before (continuous line) and after electron irradiation (dashed line) with a dose of 30 Mrad.

Examples of the morphologies obtained by redispersion of particles in the new polystyrene matrix are shown in Figure 5. Figure 5a shows the morphology of the sample containing 15 wt % of large particles, while Figure 5b shows the morphology of another sample containing 15 wt % of small particles. One can see that the CSS morphology of particles is well preserved in both samples. TEM examination of numerous samples with 5 and 15 wt % particle contents revealed that particles were nearly randomly distributed across the thickness of the samples as was desired. There were, however, some instances of unavoidable clustering of particles which has, no doubt, affected the scatter in the flow stress of samples to be presented below.

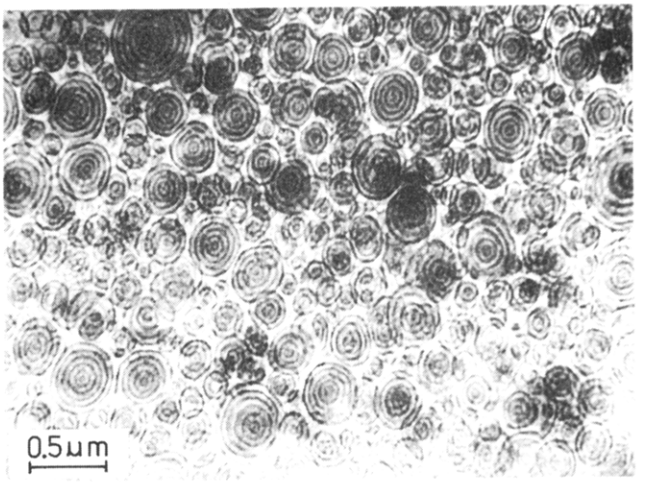

Figure 4. TEM micrograph of ultrathin film cast from a sediment collected after centrifugation of dissolved irradiated sample containing 5 wt % of KRO-1/PB-6K particles having sizes up to 0.6 µm.

SEM micrographs of large- and small-particle populations extracted from matrices and fixed with OsO_4 are shown in Figure 6. A large number of such micrographs were examined and used to determine the size distributions of particles. The normalized frequency distributions of the number and volume fraction of particles according to size of the large-particle population are depicted in Figure 7a together with the normalized cumulative distribution

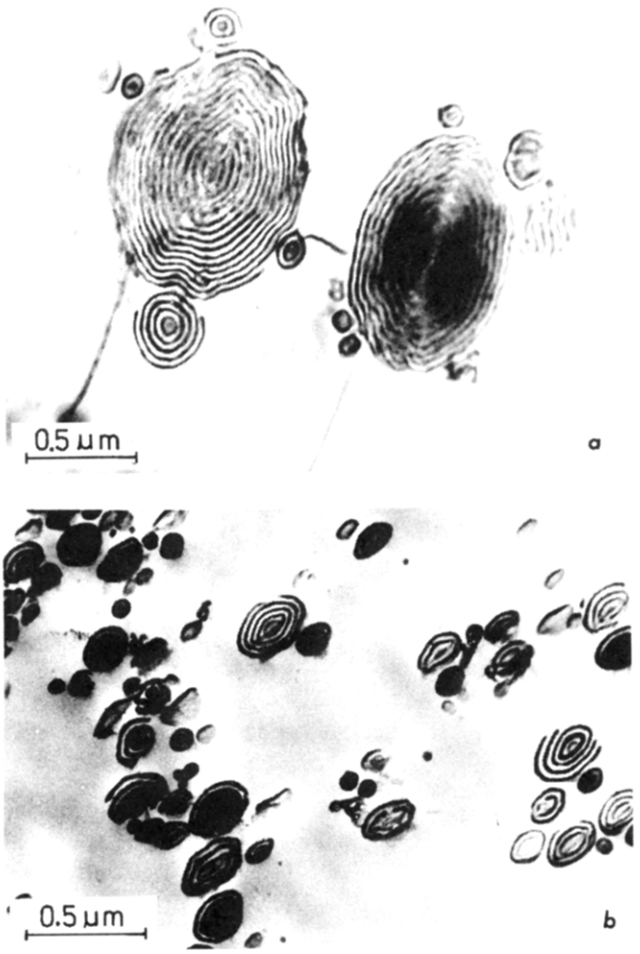

Figure 5. TEM micrographs of ultrathin sections of blends containing 15 wt % of particles: (a) large particles; (b) small particles.

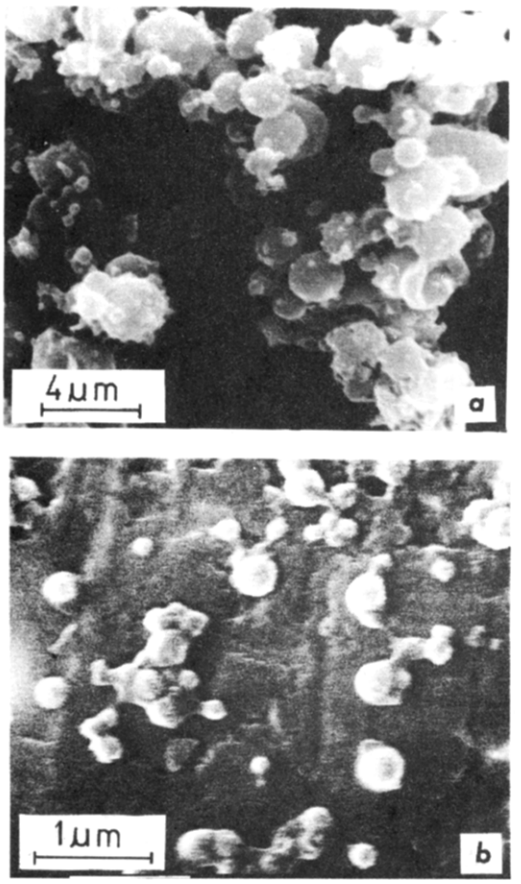

Figure 6. SEM micrographs of two populations of particles fixed with OsO_4 and separated from the PS matrix: (a) large particles; (b) small particles.

of particles having a given size or larger. The majority of the total volume of particles (ca. 70%) had diameters within the range 1.5–3.0 μm. The maximum size did not exceed 4.0 μm, with a population average size of 2.3 μm. The particles of diameter <0.5 μm, although numerous, made up only 1% of the total volume fraction of particles. The size distributions of the small-particle population are shown in Figure 7b. Here the majority of the volume fraction of particles (ca. 80%) were distributed within the diameter range 0.2–0.5 μm. The small-particle population had a maximum particle diameter of 0.6 μm, with a population average of 0.32 μm. The maximum sizes of particles as measured from SEM micrographs were in agreement with TEM observations for both particle populations.

2.2. Tensile Properties of Reassembled Blends. The results of tensile tests conducted on the reassembled samples having 5 and 15 wt % of large particles are shown in Figure 8. In Figure 8a for the case of the blend with 15 wt % of large particles, a pronounced yield point is seen around 10 MPa with the onset of plastic deformation followed by only slight increase of the flow stress. The maximum strain to fracture achieved in this case was 0.50. The blend containing 5 wt % of large particles shown in Figure 8b had yield stresses in the range 15–20 MPa and maximum strain to fracture of 0.09; however, the yield point was less pronounced than for the case of samples with 15 wt % of large particles. The blend containing 15 wt % of small particles shown in Figure 8c had a yield stress of around 19 MPa and maximum elongation of 0.13. The decrease of the content of small particles to 5 wt % changes the overall behavior of the material; the stress–strain curve for this material shown in Figure 8d exhibits a yield stress of about 25 MPa and considerable strain hardening. The maximum strain to fracture achieved was around 0.10, but is only about half of this value in the average behavior.

Figure 9 shows a light micrograph of the gauge region of the blend with a 5 wt % of large particles, obtained after fracture. This micrograph, which is typical of all blends, shows a relatively uniform distribution of whitened intense craze zones. As might be expected in the samples with 15 wt % the whitening was more uniform and less patchy.

TEM examination of the deformed sample having 15 wt % of large particles showed numerous crazes associated with particles as is shown in Figure 10a. The particles show a distorted structure. Since such distortion was not visible in samples before deformation, it is most probably a result of the combination of accumulated damage from deformation of material to final microtoming of deformed samples. A more detailed picture of crazes and particle morphology after deformation is seen in Figure 10b.

TEM examination of the deformed sample having 5 wt % of large particles revealed also crazes originating from particles. The particles were not visibly distorted as in the case of a sample having 15 wt % of large particles, due to significantly lower elongation in the former.

Figure 11a shows a micrograph of the deformed sample containing 15 wt % of small particles. Only three crazes are seen on the micrograph. Crazes that are long and straight are seen to interact with particles on their path. Careful examination of several ultrathin sections has led to the conclusion that the majority of particles did not initiate crazes. The blend containing 5 wt % of small

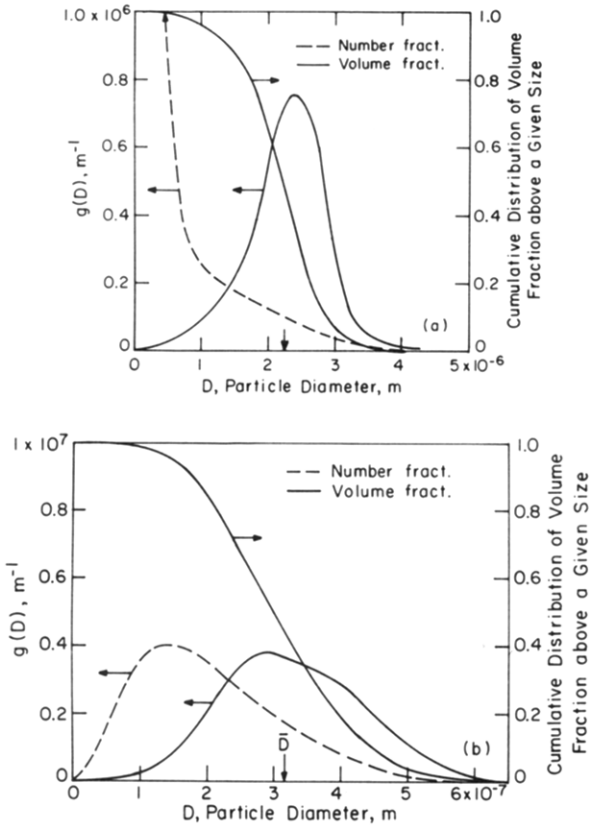

Figure 7. Normalized frequency distributions of particle numbers and volume fractions according to particle diameter with associated cumulative distributions of particle volume fractions with sizes equal to or larger than a given size: (a) for large-particle population; (b) for small-particle population.

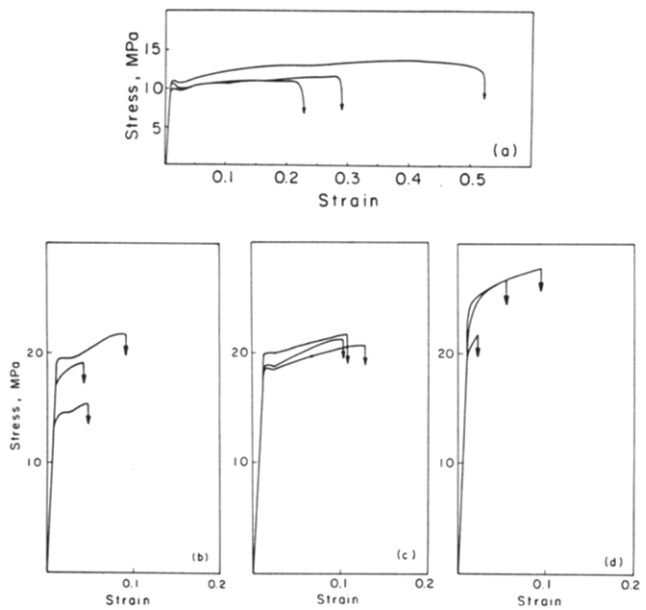

Figure 8. Stress–strain curves of blends containing KRO-1/PB-6K particles: (a) 15 wt % of large particles; (b) 5 wt % of large particles; (c) 15 wt % of small particles; (d) 5 wt % of small particles.

particles revealed a similar picture of particles not initiating crazes, as shown in Figure 11b. Here, too, the crazes were long and straight and were interacting with particles in their path.

III. Discussion

3.1. Theoretical Model. 3.1.1. Potency of Craze-Initiating Particles. It is now generally known that the brittleness of unoriented flexible chain glassy polymers such as PS, PMMA, and the like results from their crazing response in tension and from the fragility of craze matter in these polymers (for more discussion see refs 13 and 14). While the craze matter of a predominantly tufty structure that forms and spreads in these polymers by an interface convolution process is now well understood,[15] what governs its fracture still remains inadequately studied (see refs 2, 13, 14, and 16). It is, however, well established that the intrinsic fracture of craze tufts by a complex statistical sequence of chain scission processes[2,16,13,14] is almost always hastened by entrapped particulate impurities that act as imperfections to trigger the fracture process prematurely.[16-18] Several approaches have been tried to toughen such brittle thermoplastic polymers. Preorienting a glassy polymer by warm stretching is known to suppress crazing[19] but is difficult to apply to complex parts. Blending noncrazable inflexible chain polymers into flexible chain polymers has been shown to be effective[20] but requires relatively large volume fractions of the inflexible chain additive. Finally, while it is in principle also possible to cleanse the polymer of the offending particulate impurities that initiate fracture in craze matter,[18] this turns out to be impractical. This leaves the lowering of the craze flow stress by promotion of craze plasticity through the incorporation of compliant particles as the preferred method, by far.[13,14]

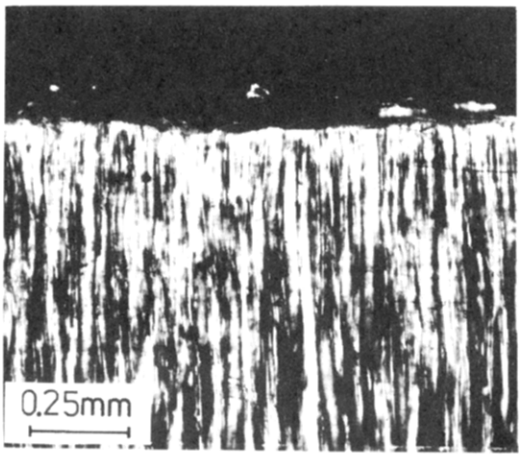

Figure 9. Light micrograph of the gauge region of a sample containing 5 wt % of large particles; after fracture of specimen.

The craze strain rate $\dot{\epsilon}$ in tension in a homopolymer can be given by a kinematic equation of the type

$$\dot{\epsilon}_p = \dot{\theta} = h\epsilon^T \rho \dot{r} \tag{1}$$

where $\dot{\theta}$ is the rate of dilatation (indicating that craze plasticity is dilatational plasticity), h is the primordial thickness of a polymer slab that transforms into a fully developed craze when it undergoes a dilatational uniaxial transformation strain of ϵ^T, ρ is the active craze front length per unit volume,[21] and $\dot{r}$ is the radial growth rate of a typical lens-shaped craze. While the kinetics of the exponentially stress dependent growth rates of crazes are now well understood,[15] there is only fragmentary understanding of what governs the active craze front length in a homopolymer,[21] beyond the qualitative knowledge that ρ depends strongly on the potency of initiating sites of crazes. Normally in single-phase homopolymers crazes are initiated almost exclusively from surface imperfections. These, while probably potent, are too few and cannot result in plastic behavior before crazes that emanate from them can traverse through the elastic interior. Thus, under the high stresses that are required to propagate the surface-

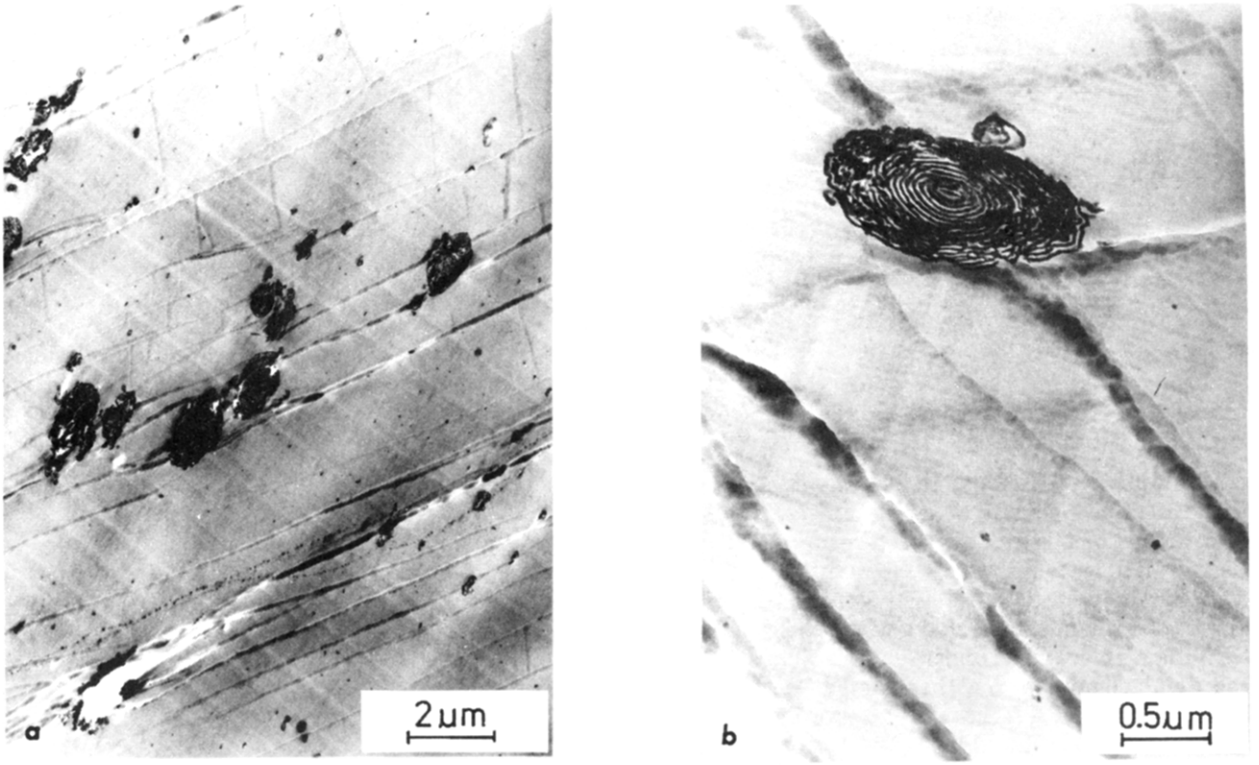

Figure 10. TEM micrographs of ultrathin sections of the deformed samples: (a) showing crazes among large particles: in a blend containing 15 wt% of particles; (b) larger magnification detail of the same in (a).

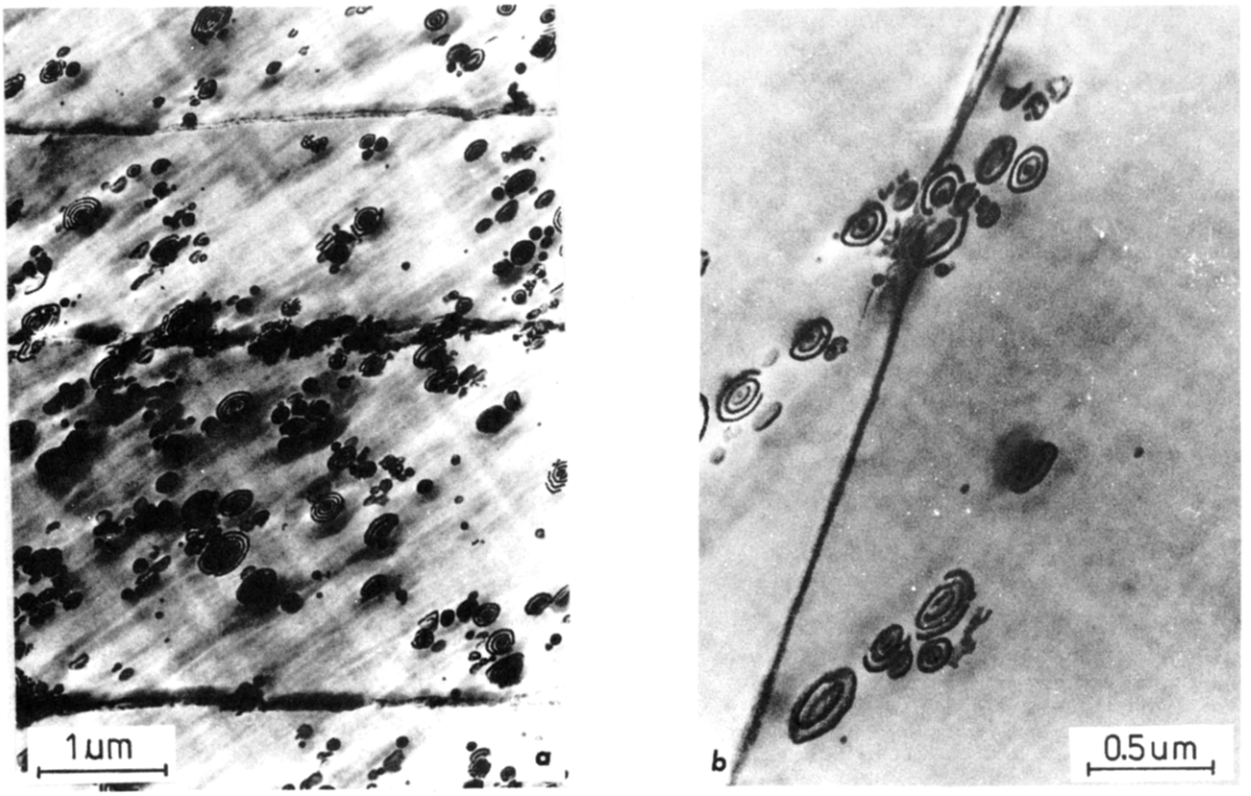

Figure 11. TEM micrographs of ultrathin sections of deformed samples containing small particles: (a) 15 wt % of particles; (b) 5 wt % of particles.

initiated crazes through the part, craze fracture occurs prematurely in a relatively short time, limiting the overall craze strain to only a few percent. On the other hand, relatively homogeneous dispersal throughout the volume of compliant particles with good craze-initiating potency can quickly establish in the stressed polymer an active craze front length per unit volume several orders of magnitude larger than what can be provided for by the usual surface imperfections. For the same externally imposed strain rate, this permits a corresponding decrease in the craze front velocity and a reduced tensile stress that could be only a fraction (0.3–0.5) of the flow stress of the unmodified homopolymer. Under such lower levels of tensile stress the developed craze matter then survives much longer, and

Table I
Properties of Composite Particles in Homo-PS[12]

	PS	KRO-1	HIPS	CSS	PB	notes
σ/σ_∞		0.407	0.643	0.645	0.735	
σ_e/ϵ_∞		1.130	1.540	1.670	1.730	
E_p, GPa	3.00	2.40	0.333	0.138	0.047	
K_p, GPa	2.50	2.28	2.18	2.05	1.50	
μ_p, GPa	1.15	0.903	0.111	0.045	0.015	
ν_p	0.3	0.325	0.475	0.489	0.495	
σ_{ce}, MPa	38	31.5	22.5	13	10	
σ_{ct}, MPa	38	32.8	22.9	21.7	20	
A	0	0.095	0.571	0.643	0.717	eq 3
B	0	0.106	0.665	0.747	0.812	eq 5
D_c, μm		10.66	0.80	0.59	0.44	eq 6

during that time a much larger fraction of the stressed polymer is filled with crazes.

3.1.2. Particle Size Effect. Gebizlioglu et al.[7] found that the critical particle size below which crazes are no longer initiated in blends with CSS particles decreases with increasing particle compliance. On the basis of this observation, Argon et al.[22] proposed a criterion for the critical particle size that states that a particle becomes too small to initiate a craze when under full load it has a stress-induced displacement misfit that is smaller than the thickness of a mature craze. This proposal, which is qualitatively similar to one advanced earlier by Bragaw,[3] has all the elements required to explain the observed effects.

In order to state a minimum particle size criterion in a relatively precise manner, we first obtain the average homogenized elastic properties of the different particles that have been previously considered by Argon et al.[12] These are listed in Table I as the average shear modulus μ_p and Poisson's ratio ν_p of the particles, alternatively as the Young's modulus E_p and bulk modulus K_p, respectively. The homogenization of the elastic properties of the heterogeneous particles by various methods of averaging the exact solutions obtained by Boyce et al.[33] have been discussed elsewhere.[12] We then consider the particles as spherical and calculate from the classical development of Goodier[23] the uniform tensile stress σ_p inside the homogenized particle in the direction of the tensile stress σ_∞ applied to the overall sample. This can be done simply by obtaining σ_{rr} at $\theta = 0$ on the particle border at $r = R$ in the Goodier solution. This stress is[23]

$$\sigma_p = \sigma_{rr}(R,0) = \sigma_\infty(1 - A(x,\nu,\nu_p)) \tag{2}$$

where

$$A = \frac{x-1}{(7-5\nu)x + (8-10\nu)} \times \left[\frac{(1-2\nu_p)(7-5\nu)x + 2(1+5\nu_p - 5\nu\nu_p)}{(1-2\nu_p)2x + (1+\nu_p)}\right] - \frac{[(1-\nu)(1+\nu_p)/(1+\nu) - \nu_p] - (1-2\nu_p)x}{(1-2\nu_p)2x + (1+\nu_p)} \tag{3}$$

and $x = \mu/\mu_p$, with all unsubscripted symbols referring to the properties of the surrounding stiff glassy polymer matrix.

For compliant particles where $x > 1$, it is found that $A > 0$, and the stress $\sigma_p < \sigma_\infty$. Under these conditions the total flexure u_r of the particle inside the cavity is

$$u_r = R\frac{\sigma_\infty}{2\mu(1+\nu)}[1 + B(x,\nu,\nu_p)] \tag{4}$$

where

$$B = \frac{(1+\nu)(x-1)}{4[(7-5\nu)x + (8-10\nu)]} \times \left[\frac{(1-2\nu_p)(19-25\nu)2x + 4(4+8\nu_p - 5\nu - 10\nu\nu_p)}{(1-2\nu_p)2x + (1+\nu_p)}\right] - \frac{[(1-\nu)(1+\nu_p) - \nu_p(1+\nu)] - (1+\nu)(1-2\nu_p)x}{2[(1-2\nu_p)2x + (1+\nu_p)]} \tag{5}$$

We note that when $x = 1$ and $\nu = \nu_p$, both A and B vanish and the medium becomes homogeneous.

We now use the results of eqs 2 and 4 to define the critical particle size that when fully load bearing (i.e., $\sigma_p = \sigma_\infty$) can accommodate just one mature craze of thickness h_c. We note from eq 2 that a compliant particle is not fully load bearing. If a circumferential craze were to form around the equator of the particle to permit it to stretch further to become fully load bearing, i.e., if the particle stress were to go from σ_p to σ_∞, according to eq 4 the particle stretch would go from $u_r(\sigma_p)$ to $u_r(\sigma_\infty)$, where the additional stretch would have to equal half the craze thickness h_c. This gives immediately the cutoff particle size D_c:

$$D_c = \frac{h_c}{\sigma_\infty(1+B)}\left(\frac{1-A}{A}\right)[2\mu(1+\nu)] \tag{6}$$

To define the cutoff particle size uniquely, however, σ_∞ must also satisfy the craze initiation criterion of the surrounding homopolymer. For this, the craze initiation criterion of Argon and Hannoosh[24] can be used, which can be stated as a rate expression as

$$\text{rate} = \frac{1}{t_i} = C_i \exp\left\{\frac{3\sigma}{2QY} - \frac{C_2}{\sigma_e}\right\} \tag{7}$$

where t_i is the craze initiation time and σ and σ_e are the local negative pressure and equivalent tensile stress (von Mises stress) in the surrounding homopolymer, induced by the applied tensile stress σ_∞. Moreover, C_1, C_2, and Q are material constants, which for PS at room temperature are $C_1 = 1.66 \times 10^7$ s^{-1}, $C_2 = 1.65$ GPa, and $Q = 0.0133$ as obtained from biaxial craze initiation experiments by Argon and Hannoosh,[24] while Y is the tensile plastic resistance of the homopolymer, which can be taken as 70 MPa for PS at room temperature based on compression yield experiments and the known pressure dependence of the flow stress.[12,24]

3.1.3. The Craze Flow Stress. Figure 8 shows that the effect on the stress–strain behavior of different particle sizes and different volume fractions of particles is quite profound. The variations in the flow stress and the strain to fracture from sample to sample represent the variability encountered in such experiments due to variability in the particle volume fraction and distribution. It can be noted in general that for a given particle size a decrease in the volume fraction of particles increases the flow stress markedly. Moreover, for the two different particle populations of small particles having an average particle size of 0.32 μm and of large particles with an average size of 2.3 μm, the flow stress is markedly higher for the samples with the small particles than for the samples with the large particles. Similar results have also been obtained by Dagli et al.[25] on a parallel study using particles of HIPS. Thus, a general explanation of these effects is needed.

To explain these results we develop a simple flow stress equation based on a different form of the kinematical equation of the craze strain rate given in eq 1. For the application of craze plasticity where the particles play a

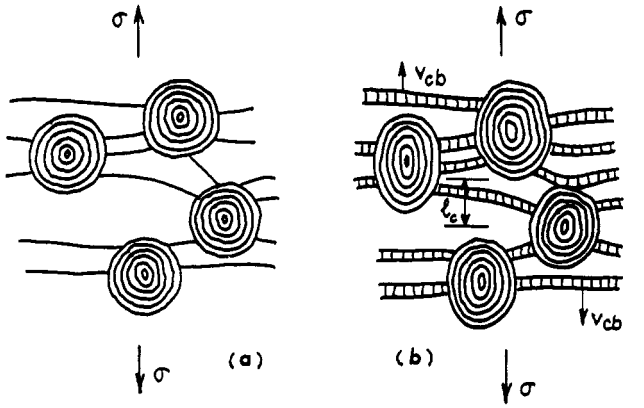

Figure 12. Sketch showing an idealized distribution of crazes among an equivalent set of cylindrical (plane strain) compliant particles: (a) at the beginning of deformation, where crazes are established but are very thin; (b) in the well-developed flow range.

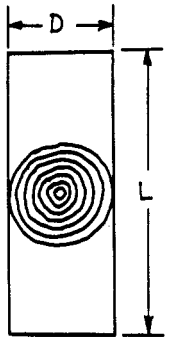

Figure 13. Sketch of the assumed periodic cell of one equivalent cylindrical particle and its surrounding.

primary role, we reinterpret this equation in a simpler way by considering that a network of thin crazes forms between the particles to establish a steady-state density of craze interfaces which subsequently merely translate in the direction of the applied stress to convert more polymer into craze matter as sketched out in Figure 12. In this model eq 1 acquires a slightly different form to become

$$\dot{\epsilon}_p = 2\frac{\epsilon^T v_{cb}}{l_c} \tag{8}$$

where ϵ^T ($=\lambda - 1$) is the uniaxial craze transformation strain (which can be taken as $\epsilon^T = 4.0$ for homo-PS), v_{cb} is the velocity of the craze border under a tensile stress acting across it, and l_c is the mean distance between widening crazes: the factor 2 arises because presumably each craze will have two active interfaces that can move simultaneously in opposite directions. To determine the mean distance l_c between active crazes consider a statistically equivalent plane strain model of randomly positioned cylindrical particles. Then as Figure 13 shows, the mean vertical distance L between such particles is

$$L = \frac{\pi \bar{D}}{4f} \tag{9}$$

where $\bar{D}$ is the average particle diameter and f is the volume fraction of particles. [In the experiments what was controlled was the weight fraction and not the volume fraction. In these systems, however, the difference between volume fraction and weight fraction is small.] Since each particle with a diameter larger than the critical cutoff diameter D_c can form n crazes, where $n = \bar{D}/D_c$, we have

$$l_c = L/n \tag{10}$$

and

$$\dot{\epsilon}_p = \frac{8\epsilon^T f}{\pi D_c} v_{cb} \qquad (D > D_c) \tag{11}$$

where we assume that the stress dependence of the craze border velocity v_{cb} is of the same form as that of the craze tip, advanced by Argon and Salama;[15] i.e.

$$v_{cb} = \alpha v_0 \frac{\hat{Y}}{\sigma_\infty} \exp\left\{-\frac{B}{kT}\left[1 - \left(\lambda_n' \frac{\sigma_\infty}{\hat{Y}}\right)^{5/6}\right]\right\} \tag{12}$$

In this expression $\hat{Y} = 0.133\mu/(1-\nu)$ is an athermal tensile flow stress, and the other terms v_o, B, and λ_n' are a pre-exponential factor, an activation energy, and an effective craze extension ratio, respectively, all determined for the longitudinal growth of crazes. For PS at room temperature they have the values of $v_o = 1.23 \times 10^6$ cm/s, $B/kT = 44.72$, and $\lambda_n' = 1.853$.[19] The proportionality constant α in eq 12 relates the longitudinal velocity expression to one of the velocity of the border of a widening craze.

For very small particles where a significant fraction of the particle population may have diameters less than the critical cutoff size, a correction must be introduced for this effect to replace f with $fI(D_c)$, where $I(D_c)$ is the fraction of the particle population having a diameter equal to or larger than D_c; i.e.

$$I(D_c) = \int_{D_c}^{\infty} g(D)\, dD \tag{13}$$

This then gives a modified equation for the strain rate that has the final form

$$\epsilon_p = \frac{8\epsilon^T f}{\pi D_c} I(D_c) v_{cb} \tag{11a}$$

where D_c is given by eq 6. Dagli et al.,[25] who have successfully adopted the strain rate expression of eq 11a to explain the particle size and volume fraction effects on the craze flow stress in a very similar study on HIPS, have shown that the constant α in eq 12 should have a value of 0.282.

Equation 11a can now be taken as the characteristic equation for the flow stress and, upon substitution of eqs 6 and 12 into it, can be inverted to solve for the craze flow stress σ_∞ to obtain

$$\sigma_\infty = \frac{\hat{Y}}{\lambda_n'}\left[1 - \frac{kT}{B}\ln\left(\frac{8\alpha\epsilon^T f A(1+B)\hat{Y} I(D_c) v_0}{\pi(1-A)h_c \dot{\epsilon}_p E}\right)\right]^{6/5} \tag{14}$$

where E is the Young's modulus and $\dot{\epsilon}_p$ is the imposed machine strain rate. It is to be recalled that when a significant fraction of the particle sizes lies below the critical cutoff size D_c, which is stress dependent, then $I(D_c)$ can be significantly less than unity and solution of eq 14 for the flow stress has to be carried out implicitly by finding a simultaneous solution of it together with eqs 6 and 13. This will be needed for the population of small CSS particles considered in this study as we will see below.

3.2. Comparison with Experiments. 3.2.1. The Cutoff Particle Size. Before we discuss the specific experimental results of the present investigation, related particularly to the stress–strain curves of Figure 8, we compare the predictions of eqs 6 and 7 with experimental results summarized by Argon et al.[12] In Table I the stress-concentrating characteristics of particles made of KRO-1 resin and those of the HIPS and CSS morphology are given together with a particle made up of pure PB rubber.[12] The table gives the local equatorial concentration of negative

pressure σ, and equivalent tensile stress (von Mises stress) σ_e, produced by an applied tensile stress σ_∞, as well as the experimentally measured craze yield stresses σ_{ce} in PS containing such particles at a volume fraction of 0.22. No particle interactions were considered since the application of the developments were intended for particle volume fractions of 0.05 and 0.15. For such relatively dilute levels of particle filling such interactions are unimportant (making no more than a 5% change) as has been discussed in some detail by Boyce et al.[33] It is useful to point out further that with the exception of the pure PB particles where thermal misfit stresses are substantial, such stresses are relatively unimportant in the KRO-1, HIPS, and CSS morphologies.[33] Therefore, they have been ignored here.

For the values of C_1, C_2, Q, and Y given above in connection with eq 7, for PS at room temperature, we calculate first from this equation a normalized reaction constant ln (t_iC_1) of 23.0 for homo-PS for the observed craze yield stress of σ_{ce} = 38 MPa. With this reaction constant and the stress concentration factors given in Table I, we calculate the theoretical tensile craze initiation stresses σ_{ct} for KRO-1, HIPS, CSS, and PB particles. These are also listed in Table I. We note that the theoretical craze initiation stresses of KRO-1 and HIPS compare very well with the experimental values while the values calculated for CSS and PB particles are a factor of about 2 too high. It has now been established conclusively[26-28] that the unusually low experimental craze stresses of material with CSS and PB particles is due to a new phenomenon of contained-solvent crazing resulting from the plasticizing effect of the presence of free rubber precipitated out in the PS. From this, we conclude that if this phenomenon had not been present, the craze yield stresses of the material with CSS and PB particles should indeed be close to the calculated values σ_{ct} given in Table I.

Next we use the calculated craze initiation stresses in eq 6 to explore the particle size effect. As a standard of comparison we take the HIPS particles for which the critical particle size for craze initiation at the craze yield stress has been established experimentally to be 0.8 μm.[10] From eq 6 we calculate, for the values given in Table I, the thickness h_c of a mature craze. This is found to be $h_c = 1.36 \times 10^{-6}$ cm, a value that is of the order of some of the thinnest crazes that have been reported. With this calculated value of h_c we determine the critical particle sizes of KRO-1 resin, CSS, and pure PB. These are listed also in Table I. Of these the predicted value of the critical cutoff particle size for KRO-1 is in excess of 10.66 μm, confirming that this particle must become very large indeed before it can initiate crazes. On the other hand, the critical particle sizes of CSS and pure PB morphologies are found to be 0.59 and 0.44 μm, respectively. For the CSS particle the calculated value is ca. 4.5 times larger than the value reported by Gebizlioglu et al.[7] that was thought to initiate crazes. Since the judgment for craze initiation of the above authors was based on the observation of a particle surrounded by a craze, which could have been a result of the craze striking the particle rather than being initiated by it, we do not consider this disagreement serious. In fact, a more direct extrapolation of the plots of the above authors of the particle size dependent craze propensity which cuts off the very low tail of their curve gives a minimum particle size of 0.45 μm for the CSS particles. This is much closer to the predicted value given above.

3.2.2. The Craze Flow Stress. We next determine the level of the craze flow stress by evaluating eq 12 for the four different reassembled blends containing the small particles and the large particles at volume fractions of 0.05 and 0.15, respectively, for each case.

Table II
Craze Flow Stresses of the Four Reconstituted Blends (MPA)

	f = 0.05	f = 0.15
Small Particles ($\bar{D}$ = 0.316 μm)		
σ_c(exptl)	23.3	19.1
σ_c(theor)	29.1	27.5
σ_c(theor adjusted)	19.9	18.8
Large Particles ($\bar{D}$ = 2.26 μm)		
σ_c(exptl)	17.3	10.5
σ_c(theor)	23.5	20.8
σ_c(theor adjusted)	16.1	14.2

Considering the large-particle population first, given by the distribution of particles in Figure 7a, we note that nearly the entire distribution lies above the cutoff particle size D_c shown in Table I calculated for the theoretical craze initiation stress of 21.7 MPa. Therefore, we take $I(D_c) \approx 1.0$ and calculate the craze flow stresses directly from eq 12 for the two volume fractions of f = 0.05 and 0.15 to be 23.5 and 20.8 MPa, respectively.

For the blends with the small-particle population we note, however, from Figure 7b that much of this particle size distribution lies below the critical particle size for any expected level of flow stress, requiring simultaneous solution of eqs 12, 6, and 13. This can be done operationally by trial and error by using eq 6 for any trial stress to obtain D_c and evaluate $I(D_c)$ for this D_c directly from the cumulative probability curve given in Figure 7b. As a result we obtain the craze flow stresses for volume fractions f = 0.05 and f = 0.15 to be 29.1 and 27.5 MPa, respectively. These four calculated values are entered in Table II together with the actual average experimental values obtained from Figure 8. Clearly, the calculated values for the two particle populations at the two different levels of volume fractions are in the correct order when compared with experimental measurements as can be seen from Table II. It is equally clear, however, that the experimental results are all very much lower than their corresponding theoretically calculated values for the chosen sets of properties that are characteristic of unmodified homo-PS. As already mentioned above, the CSS particles are known to incorporate a significant volume fraction of low molecular weight PB (PB-6K) which is physically trapped in the concentric shells but apparently becomes available to be drained onto the surfaces of crazes that touch and disrupt these particles, as discussed by Argon et al.[28] Hence, the low level of the craze flow stress is considered to be a local plasticization effect due to the lowering of the plastic resistance of the craze matter tufts resulting from the deformation-induced negative pressure that increases solubility of the PB in PS.[26,28] If this were indeed the case, then better agreement between the calculated values and the experimental flow stresses can be obtained by rescaling the athermal plastic resistance $\hat{Y}$, which is apparently reduced as a result of this plasticization. An optimum rescaling can be accomplished by using an average value of the four ratios of the experimental to theoretical flow stresses, i.e., 0.684. These adjusted values are also listed in Table II and should represent the effect of the plasticization-induced reduction of the effective plastic resistance of the material making up the craze matter tufts. This reduction in plastic resistance is considerably smaller that what appears in the original experiments of Gebizlioglu et al.[7] with the CSS particles. In that study a measured average value of craze flow stress was 8 MPa while the calculated value from eq 12 would give a flow stress of 19.9 MPa. Thus, in those

Table III
Properties of Block Copolymer KRO-1 and Polystyrene Lustrex HH-101 at 20 °C

	KRO-1	HH-101
M_w	179000	268000
M_n	132000	112000
density, g/cm³	1.02–1.05	1.04
weight fraction of PB	0.23	

experiments the local plastic resistance reduction factor for the material inside the craze was as large as 0.401. In the present experiments the reduction factor is only on the average 0.684. We attribute this partly to the lower molecular weight (M_w = 3000) of the PB used by these investigators and partly to the irradiation of the particles in the present study to a dose of 30 Mrad to make them resistant to the solvent processing that we discussed in section II. Evidently, this irradiation has tied down some of the PB-6K into the particle morphology and has prevented it from draining out onto the surfaces of the crazes. There is another slight difference between CSS particles used in the present study and in the studies of Gebizlioglu et al.[7] and Argon et al.[12] The PB-6K content in the CSS particles of the PB-6K/KRO-1 blend was 0.166 while the PB-3K content in the CSS particles of the PB-3K/KRO-1 blend was 0.25. Thus the total PB content in the CSS particles of the PB-6K/KRO-1 blend was 0.36 while in the PB-3K/KRO-1 blend it was 0.42. We note that while the adjustment that was made on the theoretical predictions by using the reduction factor of 0.684 has given tolerable agreement between experiments and theory, there are still considerable variations away from the adjusted values. We attribute these differences to departures of particles from complete random distributions, as, e.g., the particles in Figure 11 show.

In the related experimental study of Dagli et al.[25] where the particles were the conventional HIPS particles and were not modified in any way, the properties of the reassembled material are more nearly predictable by the theoretical model discussed above.

Acknowledgment. This research was supported primarily by the NSF/MRL through the Center for Materials Science and Engineering at M.I.T. under Grant DMR-84-18718. We are also pleased to acknowledge a partial postdoctoral fellowship from the Mobil Chemical Co. of Edison, NJ, that made the stay of E.P. at M.I.T. possible. For this fellowship support we are grateful to Drs. B. Gunesin and A. R. Hoge.

Appendix I. Experimental Procedure

AI.1. Sample Preparation. Ternary blends were prepared from polystyrene (PS), Lustrex HH-101, manufactured by Monsanto Plastics and Resin Co., polystyrene/polybutadiene block copolymer, KRO-1, manufactured by Phillips Petroleum Co., and low molecular weight polybutadiene (PB-6K) prepared by anionic polymerization in our laboratory. Characteristics of PS and KRO-1 resin are given in Table III. The PB addition had M_w = 6000 (PB-6K) and a narrow molecular weight distribution (M_w/M_n = 1.06). A base solution containing 5% by weight of polymers in toluene was prepared and filtered through a 0.2-μm pore size Millipore Fluoropore filter. The composition of polymers in solution was 95 wt % of PS, 4.166 wt % of KRO-1, and 0.833 wt % of PB-6K, which always led to well-developed CSS particles in cast films.

Two different ways of casting were utilized in the production of particles. Spin casting at 3600 rpm was conducted in an inert atmosphere provided by a constant flow of dry nitrogen at the rate 0.24 L/min. The temperature of the spin caster was maintained at ca. 40 °C for 66 h and at 100 °C for another 24 h. Further details of the spin-casting technique have been described elsewhere.[6,29] A second type of film was cast in a static way under fast air flow in a large pan made from aluminum lined with Teflon. Casting was accomplished at room temperature within 1 h.

In order to remove residual stresses as well as residual toluene, the films were vacuum annealed. They were kept in a vacuum oven at a pressure of 10^{-1} Torr while the temperature was increased to 100 °C during a 24-h period and kept there for 24 h. After annealing, samples were program cooled to room temperature during ca. 8 h still in the oven under vacuum. Samples cast in a static way at room temperature were kept for an additional 24 h under vacuum at room temperature prior to annealing, due to their higher toluene content after casting. To determine the morphologies of the samples, a piece of the sample was stained in a 1 wt % aqueous solution of OsO_4, microtomed, and examined under TEM. All particles had well-formed morphologies of concentric spherical shells of PB and PS layers.

To construct samples with particles in narrow ranges of particle sizes, the initially cast films were used as sources of CSS particles by dissolving away the PS matrix and collecting and sorting the particles for later incorporations into new blends.

To separate the particles from the surrounding PS matrix, a procedure based on irradiation of films, dissolution, and centrifugation was devised. To give the particles enough mechanical integrity to survive direct manipulation, the PB in the particles was irradiated to produce some cross-linking. Electron irradiation is a convenient means for such cross-linking of PB for this purpose.[30] Since PS is much less sensitive to irradiation than PB, it was possible to cross-link the PB phase in particles without significant cross-linking of the PS matrix. It was necessary to carefully limit the irradiation dose to provide enough strength to the particles without significant effects on their flexibility or on the solubility of the PS matrix in solvents. To find the optimum conditions for irradiation the spin-cast samples were stacked into 2-mm sandwiches and irradiated with 2.5-MeV electrons to doses of 2, 5, 10, 20, 30, 40, 50, and 100 Mrad. It was found that the lowest dose which led to sufficient fixation of the morphology of the particles and preservation of their sizes in recast samples was 30 Mrad. Higher irradiation doses, especially above 50 Mrad, caused significant increases in particle stiffness and cross-linking of the polystyrene matrix, producing microgels that could not be efficiently separated from the CSS particles. Therefore, the 30-Mrad dose was chosen for irradiation of all samples that served as sources of particles.

The irradiated samples were dissolved in toluene to a 1 wt % concentration. The solution was then centrifuged at 20 °C for 3 h at an acceleration of 96000*g*. The particles formed a gel at the bottom of the centrifuge tubes. This gel was carefully collected, immediately diluted with toluene to a concentration lower than 0.1 wt %, and agitated until completely redispersed. The morphology of the particles collected after centrifugation was examined by means of transmission electron microscopy (TEM). The TEM specimens were prepared in the form of ultrathin films by casting the particle suspension onto a support glass. The films were transferred onto transmission electron microscope grids, stained for 24 h in vapors of OsO_4, and examined in TEM. The solutions bearing particles extracted from the spin-cast samples were passed through 5-μm pore size Millipore Teflon filters to remove the largest particles and the clusters of particles that were formed during centrifugation.

The amounts of particles in suspensions were determined by solvent evaporation from several milliliters of suspension and by weighing the residues. Four different blends containing 5 and 15 wt % of particles from both sources were prepared as follows: A 5 wt % PS solution in toluene was prepared, stored overnight, and filtered through a 0.2-μm pore size Millipore Fluoropore filter. Appropriate amounts of dilute (<0.1 wt %) particle suspensions in toluene and the 5 wt % PS solution were mixed together in order to obtain bulk samples containing eventually 5 and 15 wt % of particles in a PS matrix. These homopolymer-containing suspensions were stirred slowly overnight to create uniform suspensions. Solvent was evaporated at a rate of ca. 5 mL/h under a fast flow of filtered nitrogen or argon at room temperature. During the evaporation of solvent the suspensions were stirred continuously. When the concentration of solids reached 0.5–1.0 wt %, evaporation was temporarily interrupted to allow the

suspensions to be filtered through a glass filter having pore sizes ranging from 25 to 50 μm in order to remove dust particles. Films were eventually cast at room temperature using the static-casting technique when the suspensions reached a concentration of 5 wt %. After ca. 12–15 h solidified polymer films were obtained of a 0.25–0.45-mm thickness. These films were then placed in a vacuum oven on a flat metal plate covered with a fine nylon net. The temperature of the metal plate was controlled within 1 °C, and the pressure in the oven was maintained below 3×10^{-2} Torr. The samples were held in the vacuum at room temperature for 24 h, then at 60 °C for 20–24 h, and finally for 24 h at 100 °C in order to equilibrate the structure, to relax any residual stresses, and to remove the last traces of residual solvent. Finally, the samples were slowly cooled inside the oven over a period of several hours. The tensile properties of the samples were studied, and their morphologies were examined with TEM before and after deformation.

AI.2. Morphology Examination. In order to prepare the final bulk samples containing 5 or 15 wt % of particles for TEM examination, a standard procedure was applied: A small fragment of a cast and vacuum-annealed sample was stained in a 1 wt % aqueous solution of OsO_4. The OsO_4 causes strong cross-linking and staining of the PB phase only. Ultrathin sections of a thickness around 600–800 Å were microtomed and examined under TEM.

In order to determine the size distributions of particles in the samples containing large particles, the method described by Keskkula and Taylor[31] was used with some modifications. A small fragment of the sample was brought into contact with 1 wt % solution of OsO_4 in cyclohexane, which enhances the penetration of OsO_4 into the material and fixes the particles without causing strong swelling and particle disruption. After 6–7 days in this solution toluene was added to dissolve the residual polystyrene matrix. These dilute solutions were centrifuged at $10^4 g$ for 0.5 h and the sediment was collected. Centrifugation and sediment collection were repeated several times until no further sedimentation occurred. The collected particles were resuspended in fresh toluene and subjected to ultrasonic excitation for 0.5 h to achieve better dispersion. Then a drop of suspension was placed on a suface of polished specimen holder for examination in the scanning electron microscope (SEM). After evaporation of solvent the specimen was coated with gold and examined under SEM.

In the case where only small particles were present and swelling effects were less pronounced, a different procedure was applied: 0.1 mL of particle suspension in toluene was mixed with 0.4 mL of a 1 wt % solution of OsO_4 in cyclohexane left for 4 days. During that time the suspension was occasionally shaken. Then a drop of the suspension was placed on a surface of a polished specimen holder and similarly examined in the SEM.

In order to determine the particle size distribution, the diameters of at least several hundreds of particles were measured for each sample.

AI.3. Tensile Testing. Tensile tests of cast films were performed on an Instron tensile testing machine. Oar-shaped standard specimens with 6.35-mm gauge length and a 3.18-mm gauge width were cut from films. Thicknesses of tensile specimens varied from 0.20 to 0.35 mm. Specimens were conditioned before testing in a standard laboratory atmosphere of 23 °C and 55–60% relative humidity for at least 24 h. Tensile tests were performed at a strain rate of 1.3×10^{-4} s^{-1} at room temperature.

AI.4. Morphology of Deformed Samples. The gauge region of deformed samples was examined under a polarized light microscope with crossed polarizers. The microstructure of deformed samples was examined with TEM. After fracture of the sample in a tension test, one part of the fractured sample was placed in a tensioning frame, restretched to the same strain prior to fracture, and submerged in a 1 wt % aqueous solution of OsO_4 for several days for fixation and staining in the stretched state. The OsO_4, besides staining the PB phase, also fixes and stains the craze matter.[32] Ultrathin sections were then cut from the gauge region with an ultramicrotome in a direction approximately at 45° to the principal tensile axis. The sections were cut across the thickness of the specimen at least 0.5 mm away from the lateral sample surface and at right angles to the craze planes in order to minimize artifacts due to sectioning. The ultrathin sections were examined under TEM.

References and Notes

(1) Bucknall, C. B. *Toughened Plastics*, Applied Science Publishers Ltd.: London, 1977.

(2) Kramer, E. J. In *Advances in Polymer Science: Crazing*, Kausch, H. H., Ed.; Springer: Berlin, 1983; Vol. 52/53, p 1.

(3) Bragaw, C. G. *Adv. Chem. Ser.* **1971**, *No. 99*, 86.

(4) Bucknall, C. B.; Smith, R. R. *Polymer* **1965**, *6*, 437.

(5) Schmitt, J. A.; Keskkula, H. J. *Appl. Polym. Sci.* **1960**, *3*, 132.

(6) Gebizlioglu, O. S.; Argon, A. S.; Cohen, R. E. *Polymer* **1985**, *26*, 519.

(7) Gebizlioglu, O. S.; Argon, A. S.; Cohen, R. E. *Polymer* **1985**, *26*, 529.

(8) Silberberger, J.; Han, C. D. *J. Appl. Polym. Sci.* **1978**, *22*, 599.

(9) Boyer, R. F.; Keskkula, H. In *Encyclopedia of Polymer Science and Technology*, Bikales, N., Ed.; Interscience: New York, 1970; Vol. 13, p 375.

(10) Donald, A. M.; Kramer, E. J. *J. Appl. Polym. Sci.* **1982**, *27*, 3729.

(11) Hobbs, S. Y. *Polym. Eng. Sci.* **1986**, *26*, 74.

(12) Argon, A. S.; Cohen, R. E.; Gebizlioglu, O. S. In *Mechanical Behavior of Materials—V*; Yan, M. G., et al., Eds.; Pergamon Press: Oxford, 1987; Vol. 1, p 3.

(13) Argon, A. S. In *Advances in Fracture Research*, Salama, K., et al., Eds.; Pergamon Press: Oxford, 1989; Vol. 4, p 2661.

(14) Argon, A. S.; Cohen, R. E. In *Advances in Polymer Science: Crazing—II*; Kausch, H. H., Ed.; Springer: Berlin, 1990; Vol. 91/92, p 302.

(15) Argon, A. S.; Salama, M. M. *Philos. Mag.* **1977**, *36*, 1195.

(16) Murray, J.; Hull, D. *J. Polym. Sci., Polym. Phys. Ed., Part A-2* **1970**, *8*, 1521.

(17) Murray, J.; Hull, D. *J. Polym. Sci., Part B: Polym. Lett.* **1970**, *8*, 159.

(18) Yang, C.-M.; Kramer, E. J.; Kuo, C. C.; Phoenix, S. L. *Macromolecules* **1986**, *18*, 2010.

(19) Rabinowitz, S.; Beardmore, P. In *CRC Critical Reviews in Macromolecular Science*, Baer, E., et al., Eds.; CRC Press: Cleveland, OH, 1972; Vol. 1, p 1.

(20) Wellinghoff, S. T.; Baer, E. *J. Appl. Polym. Sci.* **1978**, *22*, 2025.

(21) Argon, A. S.; Cohen, R. E.; Gebizlioglu, O. S.; Schwier, C. E. In *Advances in Polymer Science: Crazing*; Kausch, H. H., Ed.; Springer: Berlin, 1983; Vol. 52/53, p 275.

(22) Argon, A. S.; Cohen, R. E.; Gebizlioglu, O. S. In *Toughening of Plastics—II*; Bucknall, C. B., Ed.; Plastics and Rubber Institute: London, 1984; p 21/1.

(23) Goodier, J. N. *ASME Trans.* **1933**, *55*, 39.

(24) Argon, A. S.; Hannoosh, J. G. *Philos. Mag.* **1977**, *36*, 1195.

(25) Dagli, G.; Argon, A. S.; Cohen, R. E., to be published.

(26) Brown, H. R.; Argon, A. S.; Cohen, R. E.; Gebizlioglu, O. S.; Kramer, E. J. *Macromolecules* **1989**, *22*, 1002.

(27) Gebizlioglu, O. S.; Beckham, H. W.; Argon, A. S.; Cohen, R. E.; Brown, H. R. *Macromolecules*, in press.

(28) Argon, A. S.; Cohen, R. E.; Gebizlioglu, O. S.; Brown, H. R.; Kramer, E. J. *Macromolecules*, in press.

(29) Bates, F. S.; Cohen, R. E.; Argon, A. S. *Macromolecules* **1983**, *16*, 1108.

(30) Pearson, D. S.; Skutnik, B. J.; Bohm, G. G. A. *J. Polym. Sci., Polym. Phys. Ed.* **1974**, *12*, 925.

(31) Keskkula, H.; Taylor, P. *Polymer* **1978**, *19*, 465.

(32) Gebizlioglu, O. S.; Cohen, R. E.; Argon, A. S. *Makromol. Chem.* **1986**, *187*, 431.

(33) Boyce, M. E.; Argon, A. S.; Parks, D. M. *Polymer* **1987**, *28*, 1680.